Advanced Drug Delivery Reviews 144 (2019) 78–89

Contents lists available at ScienceDirect

Advanced Drug Delivery Reviews

journal homepage: www.elsevier.com/locate/addr

Listening for the therapeutic window: Advances in drug delivery utilizing photoacoustic imaging

Colman Moore [a], Fang Chen [a,b,1], Junxin Wang [a,1], Jesse V. Jokerst [a,b,c,*]

[a] Department of NanoEngineering, University of California, San Diego, La Jolla, CA 92093, United States
[b] Materials Science and Engineering Program, University of California, San Diego, La Jolla, CA 92093, United States
[c] Department of Radiology, University of California, San Diego, La Jolla, CA 92093, United States

ARTICLE INFO

Article history:
Received 6 May 2019
Received in revised form 4 June 2019
Accepted 2 July 2019
Available online 8 July 2019

Keywords:
Photoacoustics
Ultrasound
Drug delivery
Nanoparticles

ABSTRACT

The preclinical landscape of photoacoustic imaging has experienced tremendous growth in the past decade. This non-invasive imaging modality augments the spatiotemporal capabilities of ultrasound with optical contrast. While it has principally been investigated for diagnostic applications, many recent reports have described theranostic delivery systems and drug monitoring strategies using photoacoustics. Here, we provide an overview of the progress to date while highlighting work in three specific areas: theranostic nanoparticles, real-time drug monitoring, and stem cell ("living drug") tracking. Additionally, we discuss the challenges that remain to be addressed in this burgeoning field.

Contents

1. Introduction . . . 78
2. Photothermal and photodynamic contrast agents . . . 79
3. Nanocarriers and co-loaded contrast agents . . . 80
4. Therapeutic drug monitoring . . . 81
5. Stem cell delivery . . . 82
6. Perspective and concluding remarks . . . 85
Acknowledgements . . . 86
References . . . 86

1. Introduction

One of the fundamental goals of drug delivery research is to maximize the efficacy of therapeutics while minimizing their side effects. In many cases, this is achieved by delivering a high concentration of drug to a diseased tissue site or region of interest (e.g. tumor, infection, or organ). Therefore, in both research and clinical settings, it is critical to quantify biodistribution and pharmacokinetic parameters with high precision and accuracy. Increasingly, imaging modalities are being used to obtain these measurements because they can obtain in vivo data in a non-invasive format with good temporal and spatial resolution. Furthermore, they can be used in concert with delivery vehicles that simultaneously carry both imaging and therapeutic agents.

Ultrasound, magnetic resonance imaging (MRI), positron emission tomography (PET), and single photon emission computed tomography (SPECT) are all currently used in the clinic for pre- and post-treatment evaluation [1]. These have recently been pursued pre-clinically as molecular imaging tools to monitor therapies in real time [2,3]. For example, numerous theranostic nanoparticles for MRI have been developed [4–6] that can co-deliver materials that boost T1 or T2 contrast (such as gadolinium [7], manganese [8] and iron oxide [9]) with therapeutic molecules. Similarly, radionuclides are commonly conjugated to biomolecules or drugs for probing biological processes (e.g. 2-deoxy-2-[^{18}F]fluoro-D-glucose for monitoring glucose metabolism [10]) or pharmacokinetics using the gamma radiation detectable with PET and SPECT

* Corresponding author at: Department of NanoEngineering, University of California, San Diego, La Jolla, CA 92093, United States.
E-mail address: jjokerst@ucsd.edu (J.V. Jokerst).
[1] These authors contributed equally to this work.

https://doi.org/10.1016/j.addr.2019.07.003
0169-409X/

[11–13]. Ultrasound can harness the cavitation of microbubbles to increase contrast [14].

These modalities are powerful tools but face a variety of drawbacks. One of the main challenges in imaging local tissue distributions of drug molecules is achieving sensitivity to micromolar concentrations. PET, SPECT, and optical techniques are capable of this, but PET and SPECT have low resolutions (~1.5 mm), cannot provide anatomical information without CT pairing, and require ionizing radiation [15]; meanwhile, optical imaging is limited by shallow penetration depths and low clinical deployment [16]. MRI has high spatial resolution (<100 μm) but is limited in sensitivity (millimolar) without amplification strategies [17]. Finally, ultrasound can offer high spatiotemporal resolution but has low contrast—it is most commonly used in drug delivery as a tool to improve delivery via heat or cavitation [18].

While ultrasound can image structure in real-time, it can only distinguish tissue interfaces via differences in the speed of sound. In recent years, photoacoustic imaging has emerged as a technique that extends the contrast of ultrasound from the anatomical to the molecular—it augments the spatiotemporal resolution of ultrasound with the spectral contrast of optics [19]. This promising combination has spurred growth in the field over the past decade, with researchers pursuing applications in photoacoustic diagnostics/theranostics, surgery, and drug delivery [20–22].

This technique relies on the photoacoustic effect—energy from light is absorbed by a material and released as an acoustic vibration [23]. In a typical imaging event, a near-infrared (NIR) laser source is used to pulse light (1–100 ns) onto a tissue target [24]. At a molecular level, the target undergoes thermoelastic expansion which generates broadband acoustic waves detectable by conventional ultrasound transducers [25]. To date, it has been implemented in numerous hardware configurations: photoacoustic tomography and photoacoustic microscopy are the most widely used for research applications (Fig. 1) [19]. Microscopy offers excellent spatial resolution but limited depth; tomography has better penetration but less spatial resolution.

Contrast can arise from both endogenous and exogenous sources. The main sources of endogenous contrast in photoacoustic imaging are strongly absorbing molecules such as oxygenated and deoxygenated hemoglobin [26], melanin [27], lipids [28], and water. These targets have often been used to image hemodynamics [29], blood oxygen saturation [30], and cancers [31]. However, a wide variety of exogenous contrast agents—often small-molecules or nanoparticles—have also been developed for both boosting contrast and probing specific biomarkers or disease states [32,33]. From a materials perspective, the current landscape of these agents primarily consists of organic small molecules [34], inorganic nanomaterials [35], and organic nanoparticles [36,37].

2. Photothermal and photodynamic contrast agents

Photothermal and photodynamic therapy are two techniques for cancer therapy that rely on NIR irradiation. For this reason, they have frequently been combined with photoacoustic imaging so that the NIR excitation can be used for both imaging and therapy. In photothermal therapy, nanoparticles with a high photothermal conversion efficiency are excited with a pulsed or continuous-wave laser and the generated heat is harnessed for local tissue ablation.

One of the first examples of photothermal therapy performed with nanoparticles was published by Hirsch et al. in 2003 [39]. They found that solid tumors treated with gold nanoshells would undergo irreversible tissue damage ($\Delta T = 37\ ^{\circ}C$) within 4–6 min of 820 nm laser exposure ($4\ W/cm^2$). Since then, a large body of work has been conducted on photothermal therapy with nanoparticles [40]. Furthermore, many of these particles have been used in tandem with photoacoustic imaging: Gold nanovesicles [41], quantum dots [42], graphene oxide [43], porphysomes [44], semiconducting polymer nanoparticles [45], iron

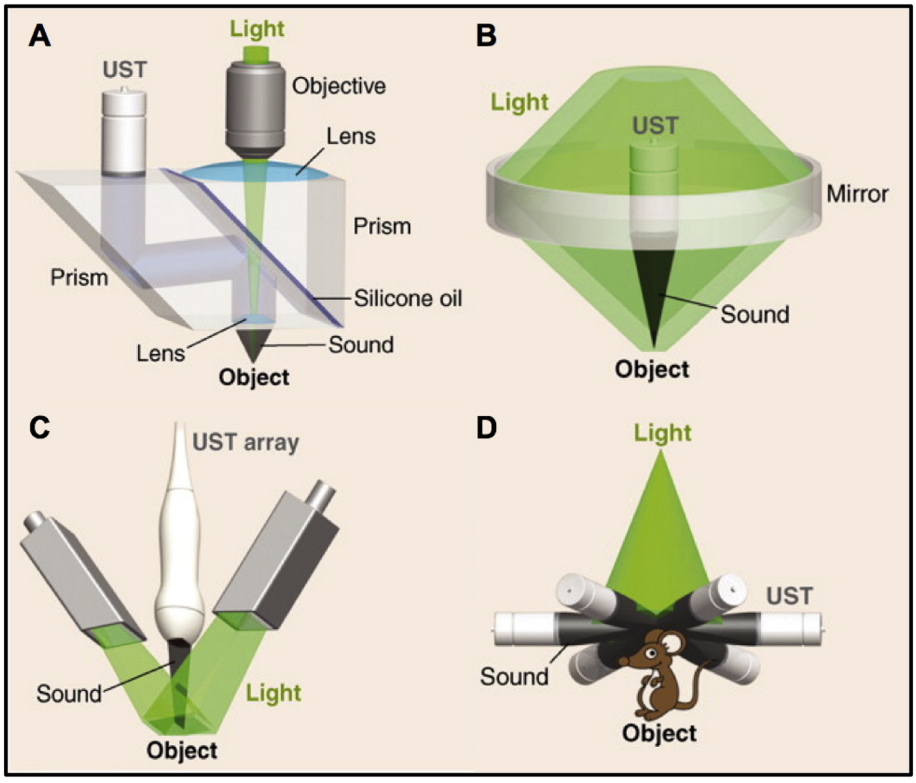

Fig. 1. Conventional hardware configurations for photoacoustic imaging. (A) Optical resolution photoacoustic microscopy (OR-PAM): a microscope objective lens is used to focus coherent excitation onto a sample while a concave acoustic lens focuses the generated acoustic wave to a broadband ultrasound transducer. (B) Acoustic resolution photoacoustic microscopy (AR-PAM): Dark-field illumination is used to focus a ring of light onto tissue while an acoustic lens focuses the generated sound to a broadband transducer. (C) Photoacoustic tomography (linear array): the excitation source is coupled to a linear array of ultrasound transducer elements. (D) Photoacoustic tomography (circular array): the excitation source is orthogonal to a circular array of transducers. Adapted with permission from [38], copyright 2012 AAAS.

oxide-polydopamine [46], and bimetallic oxide (MoMnOX) nanorods [47] are a few examples.

One unique example was demonstrated by Chen et al. in 2017; here, they synthesized nanoparticles from the temperature sensitive polymer, poly(N-isopropylacrylamide) (PNIPAM) and loaded them with gold nanorods [48]. PNIPAM shrinks when heated above its lower critical solution temperature. Therefore, when the constructs were raised above this temperature, the gold nanorods were brought closer together, resulting in plasmon coupling and a shifted absorption spectrum. When these particles were localized to subcutaneous tumors of mice, they could then be used to photoacoustically monitor photothermal therapy in real-time while reducing background from hemoglobin. Though photothermal agents are most commonly metallic, certain organic materials can also be used. These typically benefit from enhanced biocompatibility or degradability. For example, Lyu et al. recently developed a method for increasing three key properties of semiconducting polymer nanoparticles [49]. They used polymer chemistry to introduce vinylene bonds to the polymer backbone that are cleavable by peroxidase, highly expressed in immune cells. This enhanced the biodegradability in addition to the absorption coefficient (1.3-fold) and the photothermal conversion efficiency (2.4-fold).

Photodynamic therapy is an FDA-approved procedure with a track record in the clinic for treating a variety of conditions including acne [50], bacterial infections [51], and macular degeneration [52]. In the past decade, it has been increasingly studied as a cancer therapy [53,54]. Generally, the mechanism is as follows: A near infrared laser source is used to excite a photosensitizer molecule, which initiates a photochemical reaction with oxygen to produce a singlet oxygen molecule. This molecule is an unstable reactive oxygen species (ROS), possessing an opposite spin pair of electrons that make it highly destructive and cytotoxic to its local environment.

Some photosensitizers possess intrinsic photoacoustic contrast, which can allow real-time treatment monitoring. Ho et al. studied the photoacoustic behavior of five well-known photosensitizers, and found that zinc phthalocyanine produced the highest signal [55]. They subsequently showed that its localization and biodistribution could be monitored with photoacoustics in mice, revealing a peak tumor concentration at 1 h and clearing within 24 h. However, many photosensitizers do not absorb in the near infrared which limits penetration depth and compatibility with photoacoustic imaging. To address this issue, it is possible to use upconverting particles that absorb near infrared light and emit visible. Using this strategy, Idris et al. loaded mesoporous-silica-coated upconversion fluorescent particles with multiple photosensitizers for enhanced photodynamic efficacy in melanoma-bearing mice [56].

Interestingly, it is also possible to monitor photodynamic efficacy with photoacoustics by simply harnessing the endogenous contrast of blood. It is well-established that blood oxygen saturation can be directly imaged with photoacoustics via the ratiometric absorbance of oxygenated and deoxygenated hemoglobin; therefore, because photodynamic therapy requires oxygen for ROS generation, the consumption of oxygen can be monitored in real-time via the decrease in blood oxygen saturation. Shao et al. demonstrated this technique in the mouse ear vasculature using AR-PAM after tail vein injection of the photosensitizer, Verteporfin [57]. After irradiation with 80 mW/cm^2, they observed an initial decrease in the oxygen saturation followed by a gradual recovery to baseline.

Photosensitizers can also be conjugated to or loaded into photoacoustically active nanocarriers. 2-[1-hexyloxyethyl]-2-devinyl pyropheophorbide-a (HPPH) is a hydrophobic photosensitizer that has been functionalized to the surfaces of gold nanocages using a poly ethylene glycol layer; these conjugates allowed the slow release of the photosensitizer in protein-containing solutions [58]. After injection into tumor-bearing mice, the progress of delivery was monitored with photoacoustic imaging and reduction in tumor volume was observed. It is also possible for agents to be used for both photothermal and photodynamic therapy; MoS_2 nanosheets [59] and $Cu_2(OH)PO_4$ quantum dots [60] have both been investigated on this front. These quantum dots actually absorb within the second optical window (~1700 nm) making them attractive for deep tissue applications [34]. The clinical utility of these photothermal/photodynamic agents could be local administration or systemic administration to target a disease site followed by activation and treatment monitoring using near infrared excitation via photoacoustic imaging [61].

3. Nanocarriers and co-loaded contrast agents

The clinical state of the art for imaging pharmacokinetics is PET/CT with drug conjugated or co-loaded radiotracers [62]. In the preclinical space, photoacoustic imaging is being used for monitoring drug release and localized measurements of delivery. These applications require the use of in vivo sensors or co-loaded contrast agents because most small-molecule drugs do not absorb NIR light—a prerequisite for photoacoustic contrast in the body. However, it is possible for some materials such as gold nanomaterials to act therapeutically (e.g. photothermal/photodynamic therapy) while intrinsically generating photoacoustic signal. This section surveys progress in theranostic nanoparticles and materials that can act both diagnostically and therapeutically (Table 1).

Gold nanomaterials are a well-studied class of photoacoustic contrast agent due to their intense plasmon resonance in the near infrared [63]. In a study by Moon et al., hollow gold nanocages were used to encapsulate 1-tetradecanol—a material that undergoes solid to liquid transition at 38 °C (i.e., a phase-change material) [64]. The gold nanocages generated photoacoustic contrast, while external heating or high frequency ultrasound could be applied to melt the 1-tetradecanol, allowing it to diffuse out of the particles. Both methylene blue and Rhodamine 6G were dissolved in the 1-tetradecanol and shown to release from the particles at a controllable rate using this mechanism.

In 2012, Wilson et al. took advantage of perfluoropentane phase-change material to form nanodroplets that encapsulated gold nanorods for NIR absorption [65]. This is analogous to the strategy used by Hannah et al., who used perfluorocarbons to encapsulate the small molecule indocyanine green rather than nanorods [66]. Both groups found that ultrasound and photoacoustic signal could be drastically boosted following the vaporization of the droplets. Later, a group incorporated paclitaxel into the nanorod design for an activatable release scheme at laser fluence values of 14 mJ/cm^2 [67]. Zhong et al. found that indocyanine green, in addition to generating photoacoustic contrast, could act therapeutically by generating strong mechanical waves when loaded in a phospholipid-polyethylene glycol nanoparticle and exposed to constant laser fluence. They used this system for imaging and destroying cancer cells [68]. Furthermore, Kang et al. demonstrated that the photoacoustic intensity of indocyanine green could be boosted 17-fold by encapsulation in mesoporous silica nanoparticles [69]. Gold and paclitaxel have also been integrated by Manivasagan et al., who synthesized chitosan oligosaccharide gold nanospheres and loaded their surfaces with paclitaxel [70]. These showed efficacy against MDA-MB-231 cells by generating reactive oxygen species and disturbing the mitochondrial membrane potential.

Doxorubicin is another cancer drug that has been investigated by numerous groups for co-delivery with photoacoustic contrast agents. In 2014, Tian et al. synthesized rubidium tungsten nanorods, a type of transition-metal oxide nanostructure with a size dependent plasmon resonance, and loaded them with doxorubicin [71]. These particles were able to exert both chemo- and photothermal therapy (photothermal conversion efficiency: 17.8%), generating a burst drug release and localized heating following 808 nm laser exposure (1 W/cm^2) for 10 min. They were used for photoacoustic imaging and treatment of pancreatic cancer (Pance-1 tumor model) in nude mice. Other transition-metal nanomaterials that have been pursued for photoacoustic drug delivery are molybdenum oxide nanospheres; these were stabilized with polyethylene glycol and loaded with camptothecin,

Table 1
Examples of nanoparticle-based exogenous contrast agents for photoacoustic theranostics and drug monitoring.

Description	Contrast mechanism	Imaging wavelength (nm)	Therapeutic or target	Model	Reference
Perfluorocarbon encapsulated gold nanorods	Heat-induced phase transition (liquid to gas) of nanodroplets	770	Paclitaxel	Subcutaneous HeLA tumors in Balb/c mice	Zhong et al. [67]
Chitosan oligosaccharide stabilized gold nanoparticles	Thermal expansion at the peak plasmon resonance of 60 nm gold nanoparticles	532	Paclitaxel	MDA-MB-213 adenocarcinoma cells	Manivasagan et al. [70]
Porphyrinoid-loaded PLGA nanoparticles	Complexation of porphyrinoid macrocycles with uranyl cations to impart aromaticity	910	Uranium	Healthy mice with subcutaneous complexed nanoparticles	Ho et al. 2015
RB_XWO_3 nanorods	Thermal expansion of rubidium tungsten nanorods (20–40 × 5 nm)	808	Doxorubicin	Pance-1 tumor-bearing mice	Tian et al. [71]
MOS_2 nanosheets	Thermal expansion of MoS_2 nanosheets	800	Ce6 (Photosensitizer)	Subcutaneous 4 T1 tumors in Balb/c mice	Liu et al. [59]
Mesoporous silica/quantum dot coated gold nanorods	Thermal expansion of gold nanorods, leading to release of drug payload through silica layer	800	Doxurubin, p53	Subcutaneous glioma C6 tumors in Balb/c nude mice	Duan et al. [77]
Gold nanocages loaded with 1-tetradecanol (phase change)	Thermal expansion at the peak plasmon resonance of gold nanocages (60 nm side length)	750	Methylene Blue, Rhodamine 6G	Controlled release study only	Moon et al. [64]
Fucoidan/doxorubicin capped gold nanoparticles	Thermal expansion at plasmon resonance of 82 nm gold nanoparticles	532	Doxorubicin	MDA-MB-213 adenocarcinoma cells	Manivasagan et al. [70]
Intradermal optode nanosensors containing crown ether ionophores	Shifted optical absorbance following binding of lithium to chromoionophore	515, 660	Lithium	Athymic nude mice	Cash et al. [80]
Single wall carbon nanotubes with mesoporous silica/doxorubicin	Thermal expansion of nanotubes via near infrared absorbance	808	Doxorubicin	4 T1-tumor bearing mice	Liu et al. [59]

a cancer drug that could be controllably released in a mouse model of pancreatic cancer [72]. Cobalt selenide nanoplates have also been reported as chalcogenide based theranostics, exhibiting high photothermal conversion efficiency (26 °C temperature increase following 808 nm exposure for 10 min at 1 W/cm^2), low toxicity, and significant absorbance in the near infrared [73]. One of the main benefits of most metallic carriers is their ability for synergistic chemo- and photothermal therapy.

During the same year, Liu et al. loaded single wall carbon nanotubes with mesoporous silica and doxorubicin [74]. The goal was to leverage the loading and release capacity of mesoporous silica with the near infrared absorbance and photothermal conversion efficiency of the nanotubes. The researchers found that the tumor surface temperature could be increased to 48 °C when irradiated with 808 nm light at 0.5 W/cm^2 for 20 min. Again, this technique showed synergistic chemo−/photothermal effects against cancer in nude mice with 4T1 tumors. Similar efficacy and imaging traits were noted when the nanotubes were replaced with reduced graphene oxide, though the photothermal conversion efficiency is lower [75]. More recently, doxorubicin was delivered both via surface conjugation with fucoidan capped gold nanoparticles [76] and mesoporous silica-quantum dot functionalized gold nanorods [77]. This last example is particularly interesting because it included the delivery of p53 pDNA, a mechanism for gene therapy. These multi-mechanistic particles were capable of photoacoustic/magnetic resonance/computed tomography, and synergistic gene/chemo−/photothermal therapy. They could be magnetically guided to the tumor site under magnetic resonance imaging, and could be verified with photoacoustic imaging followed by activatable release via laser fluence or pH. The authors showed effective eradication and suppression of 4 T1 tumors in nude mice with this system.

4. Therapeutic drug monitoring

The high temporal resolution and contrast of photoacoustic imaging offers the potential for real-time monitoring and maintenance of drug concentrations within the therapeutic window. Therefore, there is growing interest in developing new materials in tandem with photoacoustic imaging for therapeutic assays. For example, lithium is an effective treatment for bipolar disorder between 0.6 and 1.2 mM [78], but can be toxic at high doses above 2 mM [79]. Cash et al. developed a lithium ionophore-based nanoparticle to measure lithium concentrations in 15 s using photoacoustic imaging; the binding and release of lithium cations shifted the absorption and subsequently the photoacoustic intensity of the nanoparticle [80]. This work demonstrated a novel and safe concept for chronic bipolar disorder management. In another case, porphyrinoid-containing nanoparticles were used to detect uranium ion concentrations in the parts per billion range [81]. In this case, uranium ions, though toxic rather than therapeutic, are analogous to a drug that is being monitored. Finally, photoacoustic imaging can indirectly monitor therapeutics via genetic indicators. For example, the tyrosinase-based reporter gene can catalyze the production of endogenous melanin, a strong near infrared absorber [82]. Zheng et al. found that microRNA-9, a potential gene therapy [83], could silence the translation of tyrosinase and reduce the photoacoustic signal. [84] Therefore, the photoacoustic shift could be correlated to the concentration of microRNA-9 in the cells.

To extend the capabilities of photoacoustics for monitoring drug dosing, our group has developed a photoacoustic imaging method to detect heparin. Heparin (Fig. 2A) is an indispensable surgical and cardiovascular anticoagulant with >500 million doses given annually in the world [85]. However, it is difficult to maintain safe and efficacious heparin concentrations because it has a variable molecular weight and a narrow therapeutic window [86]. Furthermore, the current heparin measurement methods, such as the activated partial thromboplastin time (aPTT) [87], anti-Xa analysis [88], thromboelastography [89], and activated clotting time [90], require lab processing and thus a long turnaround time. The maintenance of inaccurate heparin dosing due to the belated measurement results can cause severe side effects including hemorrhage and embolism [91]. Photoacoustic imaging has the potential to address this problem by rapidly and longitudinally sampling blood samples. However, the hemoglobin and deoxyhemoglobin in blood are endogenous absorbers, meaning an exogenous contrast agent is required to differentiate heparin from blood [92].

In 2016, we described a simple photoacoustic method for real-time heparin measurement in human blood [93,94]. The method employed the Federal Drug Administration (FDA)-approved dye methylene blue (Fig. 2A) as the contrast agent. It generated 31-fold enhanced photoacoustic signal when it was bound to 10 U/mL heparin (Fig. 2B). This

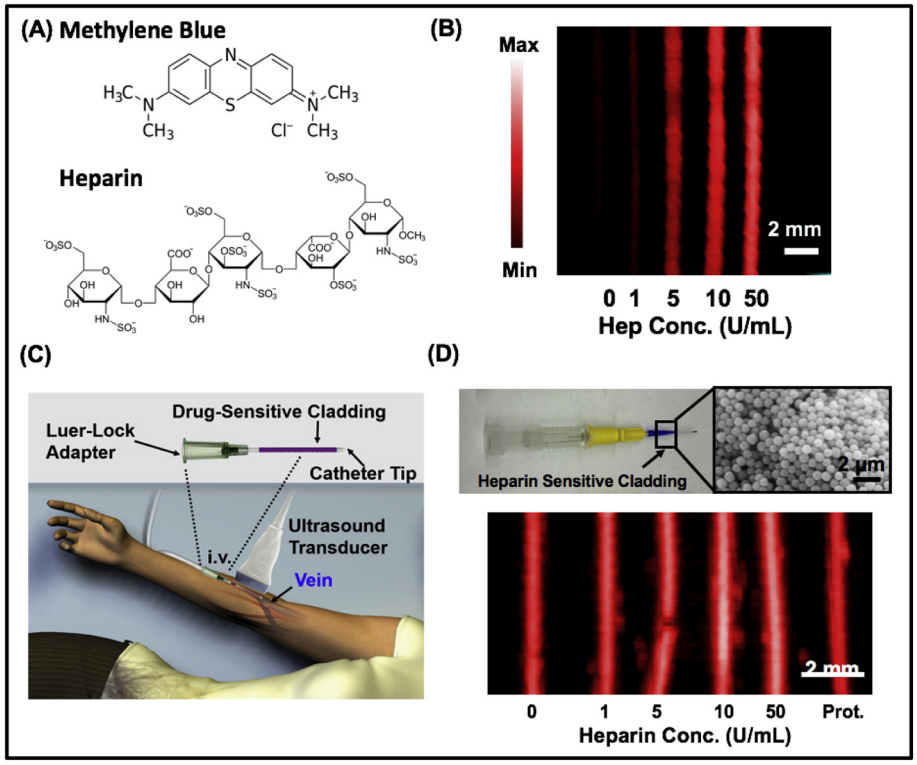

Fig. 2. Photoacoustic heparin assay. (A) The assay employs methylene blue as the contrast agent for detecting heparin in human whole blood. (B) A concentration of 0.8 mM methylene blue provided 31-fold enhanced photoacoustic signal upon addition of 10 U/mL heparin. (C) A concept illustration of catheter cladding that generates heparin contrast for clinical use. (D) This concept is demonstrated with a silica/agarose hydrogel coating that measures heparin concentrations and protamine (Prot) control. Reproduced courtesy of ACS Publications [93,94].

high contrast overcame the noise caused by other components in blood and was strongly correlated to the heparin concentrations with a logarithmic regression of $R^2 > 0.97$ and a detection limit of 0.28 U/mL. This concentration was lower than the clinical dose of heparin used in common applications including thromboembolism (7–8 U/mL), acute myocardial infarction (2.5 U/mL), and cardiopulmonary bypass (5.6 U/mL), suggesting a broad clinical potential.

The rapid and sensitive photoacoustic enhancement of methylene blue to heparin unlocked the opportunity for developing a bed-side heparin and clotting assay (Fig. 2C). Therefore, we developed a nanosensor to immobilize methylene blue on the outer surface of a peripheral venous catheter for clinical applications (Fig. 2D) [94]. The nanosensor was a silica nanoparticle/agarose hydrogel. However, simply conjugating methylene blue to the silica nanoparticle decreased the sensitivity of the photoacoustic enhancement. This was because the strong negative charges on the silica nanoparticle surface hindered the electrostatic association of methylene blue with the negative charged heparin. The photoacoustic signal could be reduced by the addition of protamine—the known antagonist of heparin.

Recently, we extended this work using the methylene blue derivative Nile Blue A infused in cellulose to measure heparin in blood samples. The cellulose sensor was a Whatman filter paper modified with polyethylene glycol for increased hydrophilicity (Fig. 3A inset). The Nile Blue A in the cellulose (0.6 nanomoles per mg of cellulose) had low solubility (< 10 ng/mL) in 0.01 M phosphate buffer saline due to ionic strength and pH, yet was highly sensitive to heparin with a detection limit of 0.28 U/mL in plasma (Fig. 3A) and 0.29 U/mL in human blood [95]. After analyzing the 78 blood samples from 16 patients that underwent cardiac ablations and received various doses of heparin, we found that the photoacoustic intensity of the cellulose sensor had strong linearity with the cumulative heparin dose (Pearson's $r = 0.85$, Fig. 3B) and the activated clotting time (Pearson's $r = 0.87$, Fig. 3C). These results suggested that the photoacoustic assay could potentially serve as a point-of-care testing method for heparin and clotting time measurement. Future work will be devoted to the development of an intravenous sensor for real-time heparin detection.

In another example, our lab used photoacoustic imaging to monitor Ag^+ delivered therapeutically (Fig. 4). Ag^+ are a well-known antibacterial agent, and Ag nanoparticles can be a reservoir of Ag^+ for targeted therapy of bacterial infections. However, there are no tools to measure Ag^+ in vivo or trigger Ag^+ release from Ag nanoparticles. Our group recently used photoacoustic imaging with gold nanorods to monitor Ag^+ release [96]. The strategy coated the gold nanorods with Ag for hybrid nanoparticles. This coating decreased their photoacoustic signal. The as-prepared, Ag-coated Au nanorods (Au/AgNRs) are stable under ambient conditions, but the addition of exogenous ferricyanide (1 mM) or endogenous reactive oxygen species results in oxidative etching of the silver shell. The photoacoustic contrast is simultaneously recovered as the silver is released, and this photoacoustic signal offers noninvasive monitoring of localized release of Ag^+.

The released Ag^+ ions showed a strong bactericidal efficacy similar to equivalent free Ag^+, and the nanoparticles killed >99.99% of both (Gram-positive) methicillin-resistant *Staphylococcus aureus* (MRSA, 32 μM Ag^+ equivalent) and (Gram-negative) *Escherichia coli* (8 μM Ag^+ equivalent). The potential of these nanoparticles was further demonstrated in a pilot rodent study. There was a 730% increase in the photoacoustic signal ($p < .01$) pre- and post- etching, and the bacterial counts in infected tissues of the treated group were reduced by 1000-fold (log CFU/g = 4.15 vs 7.75) relative to the untreated cohort.

5. Stem cell delivery

Ultrasound imaging has strong potential for guiding the injection of therapeutic stem cells ("living drugs") to specific regions because it is a real-time imaging modality and the needle tip in soft tissues can be clearly visualized under the ultrasound transducers (Fig. 5). In 2005,

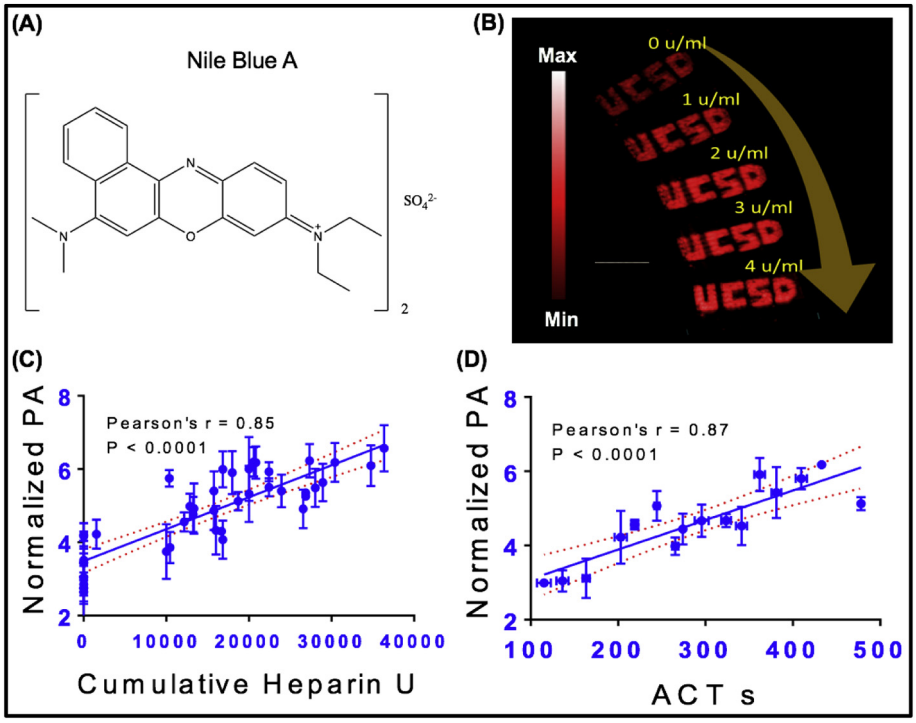

Fig. 3. Clinical validation of the cellulose sensor. (A) The photoacoustic enhancement of the cellulose sensor is a function of heparin concentration from 0 to 4 U/mL in human plasma. (B, C) The photoacoustic intensity of the cellulose sensor was correlated to the cumulative heparin doses received by the patients undergoing cardiac ablations (Pearson's $r = 0.85$) and the activated clotting time of the samples measured by the clinics (Pearson's $r = 0.87$). Panel A-C are reprinted with permission from Elsevier [95].

Springer and Rodriguez-Porcel et al. from two separate research groups described ultrasound imaging-guided percutaneous injections of cells into a mouse infarct model [97,98]. This approach is also applicable to large animals [99]. The ultrasound-guided procedure is less invasive and significantly more accurate than open-chest injections. However, it is difficult to visualize and track injected therapeutic cells with

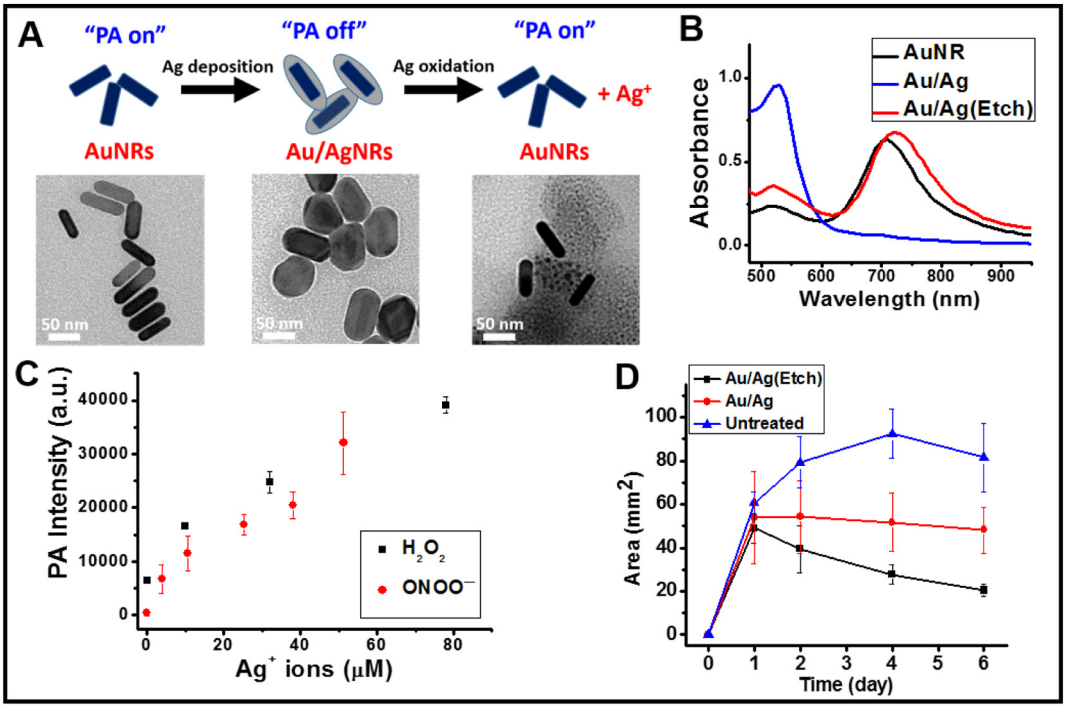

Fig. 4. Photoacoustic imaging of antibacterial silver. A, B) Gold nanorods (AuNRs) have strong infrared absorbance, which blue-shifts when they are coated with silver (Au/Ag); this decreases their photoacoustic signal. The silver can be oxidized off returning the infrared absorbance (and photoacoustic signal) while also releasing therapeutic Ag^{+}. C) This oxidation is a function of concentration of reactive oxygen species. D) This construct was used with a rodent model of methicillin resistant staph infection with significant impacts on wound size relative to controls. Reproduced with permission of American Chemical Society [96].

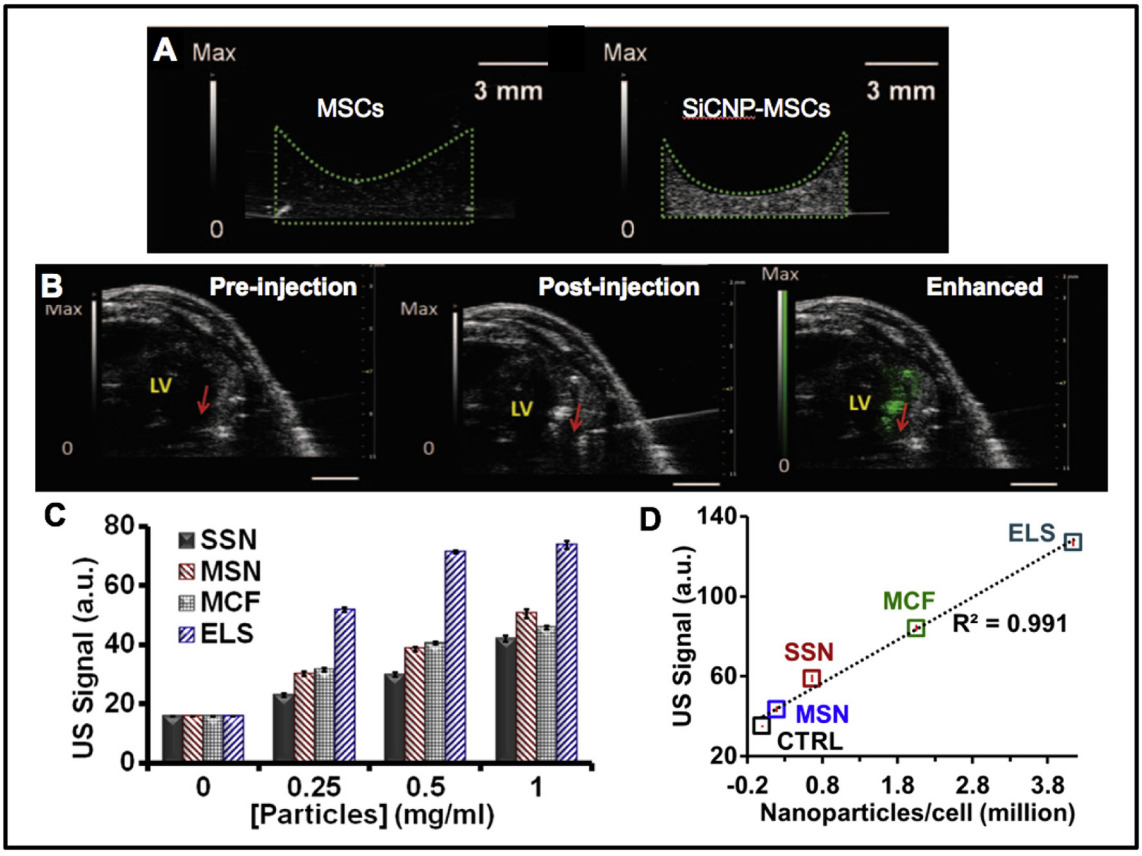

Fig. 5. Increasing ultrasound contrast of therapeutic stem cells with nanoparticles. (A) Silica nanoparticles (SiNP) enhance the ultrasound signal of MSCs. (B) SiNP-labeled MSCs are visible via ultrasound imaging after cardiac implantation. The contrast from the backscatter of SiNPs highlights the implanted cells. Green signal indicates presence of SiNP-labeled stem cells. Red arrow highlights the bevel of the needle. Panels (A) & (B) are reproduced with courtesy of the American Association for the Advancement of Science [101]. (c) Echogenicity of four types of silica nanoparticles. SSN: Stöber silica nanoparticles, MSN: MCM-41 mesoporous silica nanoparticles, MCF: mesocellular foam silica nanoparticles, ELS: exosome-like silica nanoparticles. (d) ELS showed the highest cellular uptake by hMSCs and enhanced the ultrasound signal of hMSCs the most. (c) & (d) are reproduced courtesy of the RSC [108].

ultrasound imaging because these cells have poor ultrasound contrast relative to the local tissues [100]. Moreover, the guided catheter position does not guarantee sufficient cell delivery at the desired location [101].

The inability to track stem cells leads to blindness of delivery efficiency and retention in patients [102]. However, cell tracking in vivo is essential to understanding the cell fate, therapeutic efficacy, and safety issues related to the injected cells [102]. Therefore, it is important to develop in vivo cell tracking techniques. Based on the already-existing imaging modalities, novel contrast agents can help better visualize injected cells. While contrast agents for other imaging modalities have been investigated [103], the development of ultrasound/photoacoustic contrast agents for in vivo stem cell tracking is more attractive given the convenience, low cost, and safety of ultrasound/photoacoustic imaging [104,105].

The most common ultrasound contrast agents are microbubbles. Cui et al. demonstrated that microbubbles could track neural progenitor cells in vivo [106]. An ultrasound frequency of 7 MHz could detect a single microbubble-labeled neural progenitor cell. However, the elevated ultrasound signal was only maintained for up to 7 days, close to the upper limit for microbubbles. Due to their large size and instability, microbubbles are incapable of long-term tracking for therapeutic cells in vivo [107].

Because microbubbles are limited in their utility for stem cell tracking by their short lifetimes, we have investigated silica nanoparticles as ultrasound contrast agents for therapeutic stem cell delivery and tracking; these particles are generally biocompatible and have high impedance mismatch with soft tissues.

Our group has studied the echogenicity of solid silica nanoparticles (SiNPs) [101] and MCM-41 typed mesoporous silica nanoparticles (MSNs) as therapeutic ultrasound contrast agents [109]. Both nanoparticles increased the ultrasound signal of human mesenchymal stem cells (hMSCs). The SiNP aggregated within the stem cells to amplify the ultrasound backscatter. The ultrasound contrast of SiNP-labeled hMSCs was 6 times higher than unlabeled cells (Fig. 5A). The detection limit of SiNP-labeled hMSCs in cardiac tissue of rodents was 70,000 via ultrasound imaging (Fig. 5B). The MSNs enhanced the ultrasound signal of hMSCs and increased the stem cell survival via sustained release of pro-survival agents. The detection limit of MSNs-labeled hMSCs at this concentration was near 9000 cells via ultrasound imaging. Moreover, the MSNs could degrade in cells and were cleared in approximately 3 weeks.

Later, the effect of particle morphology on echogenicity was studied for four types of silica nanoparticles including Stöber silica nanoparticles (SSN), MCM-41 mesoporous silica nanoparticles (MSN), mesocellular foam silica nanoparticles (MCF), and novel exosome-like silica nanoparticles (ELS) that are reminiscent of the shape of exosomes [108]. The porous silica nanoparticles showed stronger echogenicity than solid nanoparticles with similar diameter when their mass concentrations were kept constant (Fig. 5C). In addition, all silica nanoparticles were biocompatible with hMSCs when the labeling concentrations were no higher than 500 μg/mL. The ELS nanoparticles showed the highest cellular uptake and increased the echogenicity of hMSCs the most (Fig. 5D-E).

Another type of inorganic nanoparticle for ultrasound contrast that has been used for cell tracking are glass nanospheres. Foroutan et al. developed glass nanospheres to increase the ultrasound signal of therapeutic stem cells [110]. The nanospheres are biocompatible and

biodegradable, and thus they can be easily metabolized in the body. The glass nanosphere-labeled MSCs could be measured with ultrasound imaging with cell counts as low as 4000.

One limit of these nanoparticles-based ultrasound contrast agents is that the ultrasound signal does not reflect information about cell death. However, research involving gene editing makes it possible to specifically track live cells via ultrasound. Kuliszewski et al. programmed therapeutic stem cells to produce a specific cell surface protein H-2Hk, which is the target of the injected microbubbles [111]. Hence, only cells that have the unique cell marker will show strong ultrasound signal. Shapiro's group reported biogenic gas nanostructures as ultrasonic molecular reporters [112–114]. However, this method has only been applied in microorganisms up to this point.

While the ultrasound intensity of therapeutic cells can be enhanced by novel contrast agents, the modality still suffers from low signal-to-noise due to the lack of spectral contrast. To combat this, photoacoustic imaging combines the benefits of ultrasound and optical imaging, providing spectral contrast between targets (e.g. labeled stem cells) and local tissues [105]. Thus, photoacoustic imaging for therapeutic stem cell tracking has been more broadly investigated than traditional ultrasound imaging [111,115–117].

Gold nanoparticles are some of the most popular photoacoustic contrast agents due to their high absorption cross sections and multiplexable absorption peaks [105]. Jokerst et al. labeled MSCs with silica-coated gold nanorods and could track the labeled MSCs via photoacoustic imaging (Fig. 6A) [115]. The silica shells stabilized the photoacoustic signal of gold nanorods and increased cellular uptake. The simultaneous ultrasound and photoacoustic imaging provided clearly defined anatomic features and localization of implanted labeled MSCs. Nam et al. labeled stem cells with gold nanotracers and could track these cells via ultrasound/photoacoustic imaging after injection into the lateral gastrocnemius muscle of a rat 5 mm under the skin [118]. The same group labeled therapeutic stem cells with gold nanoparticles for treatment of neurodegenerative diseases. The detection limit of these labeled stem cells in the spinal cord was 1000 cells [117].

Prussian blue nanoparticles are another emerging class of photoacoustic contrast agents due to their strong optical absorption in the near-infrared region. We developed poly-L-Lysine (PLL)-coated Prussian blue nanocubes to label hMSCs (Fig. 6B) [119]. The PLL coating reduced the negative charge of the Prussian blue nanocubes and facilitated cell internalization. The labeled hMSCs showed strong photoacoustic contrast when imaged at 730 nm, which allowed photoacoustic imaging-guided delivery of these therapeutic cells into the desired locations. The labeled hMSCs were still detectable with photoacoustic imaging two weeks after cell implantation. The detection limit of these labeled hMSCs through the skulls of rodents was 200 cells/μL.

Organic nanoparticles have also been investigated as cellular photoacoustic contrast agents. For example, we developed an iron oxide- and 1,1′-dioctadecyl-3,3,3′,3′-tetramethylindotricarbocyanine iodide (DiR)-loaded poly(lactic-*co*-glycolic acid) (PLGA) nanobubble for trimodal ultrasound/MRI/photoacoustic imaging [120]. These nanobubble-labeled hMSCs had a 3.8-fold ultrasound and 10.2-fold photoacoustic contrast in cardiac tissue compared to unlabeled hMSCs. These nanobubbles were also visible with magnetic particle imaging, an emerging imaging modality.

Melanin nanoparticles are another class of promising photoacoustic contrast agents. These particles have great potential in translation because they are natural components of food-grade cuttlefish ink [121]. We recently reported synthetic melanin nanoparticles as photoacoustic contrast agents for therapeutic stem cell imaging [122]. The photoacoustic intensity at 720 nm of these nanoparticles could be enhanced up to 40-fold by gadolinium doping (Fig. 6C). These nanoparticles were biocompatible and could be internalized and with hMSCs. The nanoparticles-labeled hMSCs had a detection limit of 23,000 cells in vitro.

To increase the penetration depth of photoacoustic imaging, Yin et al. developed organic semiconducting polymer nanoparticles for photoacoustic tracking of therapeutic stem cells in the second near-infrared window [123]. The signal-to-noise ratio was increased compared to excitation in the first near-infrared window (Fig. 6D). These polymer nanoparticle-labeled hMSCs showed 40.6- and 21.7-fold higher photoacoustic intensity in subcutaneous and brain imaging than unlabeled hMSCs.

Researchers have developed many ultrasound/photoacoustic contrast agents for therapeutic cells delivery. However, most reported contrast agents can only provide information about the location of the implanted labeled cells with limited information about the cell number in vivo. It is possible that photoacoustic reporter gene techniques may overcome some of the existing limitations, especially ones that leverage dyes with existing FDA approval [124]. Nevertheless, tremendous and revolutionary research on multiple imaging modalities and contrast agents is still needed to fully understand the therapeutic efficacy and cell fate of stem cell therapies [102].

6. Perspective and concluding remarks

One of the remaining challenges for theranostic photoacoustic delivery systems is to improve the signal-to-background ratio [125]. For many of these systems, the signal does not change if the drug is released or not. The ability to quantify released vs. unreleased drug in vivo would be a highly valuable tool for researchers and clinicians alike. Future strategies will likely use activatable probes to address these questions [126]. When it comes to clinical deployment of nanoparticle contrast agents, the distinctions between inorganic and organic particles must also be considered. Inorganics have useful optical and magnetic properties that can be tuned by adjusting their size, morphology, and chemical composition [35]. Furthermore, their surfaces can be functionalized with both targeting and drug molecules. Due to effects such as plasmon resonance, they can drastically enhance contrast relative to most organic molecules and particles. However, organic nanoparticles (such as liposomes, micelles, and polymeric nanoparticles) offer better biodegradability; they are also ideal for encapsulating drug and targeting molecules [127]. In addition, recent progress suggests that certain semiconducting nanoparticles may match or even exceed the optical advantages of inorganics [36,45,49].

Both types of these particles have recently been explored for imaging in the second optical window ("NIR-II", 1000–1700 nm), a promising strategy that has followed the developments of NIR-II optical imaging [127]. These longer wavelengths can penetrate more deeply through tissue due to reduced scattering and autofluorescence [128]. In addition, the lower energy photons can be used with higher fluence, which is dictated clinically by the maximum permissible exposure (MPE) [129]. Some initial materials for NIR-II photoacoustics have included plasmonic metal nanoparticles, copper sulfide particles, semiconducting polymer nanoparticles, and small molecules [130–133]. Still, certain challenges must be overcome: For example, photoacoustic imaging systems must implement longer wavelength lasers, the absorbance of water at 1450 nm must be avoided, and few existing organic compounds absorb above 1064 nm [134]. Nevertheless, we will likely continue to see progress in the second optical window (1000–1700 nm) for increased penetration depths. This trend has already emerged in the field of optical imaging [128,135].

Photoacoustic stem cell delivery may benefit in the future from genetically encodable chromophores; these can allow direct visualization of target tissue or the therapeutic response with extremely high specificity [136]. Bacterial reporters such as bacteriochlorophyll a, which change their spectral signature in response to cellular activity, may also prove useful in the future for photoacoustic monitoring of gene/drug delivery [137]. Finally, achievable strategies that answer questions about drug fate relative to drug carrier will likely continue to have value. Hardware advances such as more affordable excitation sources (LEDs,

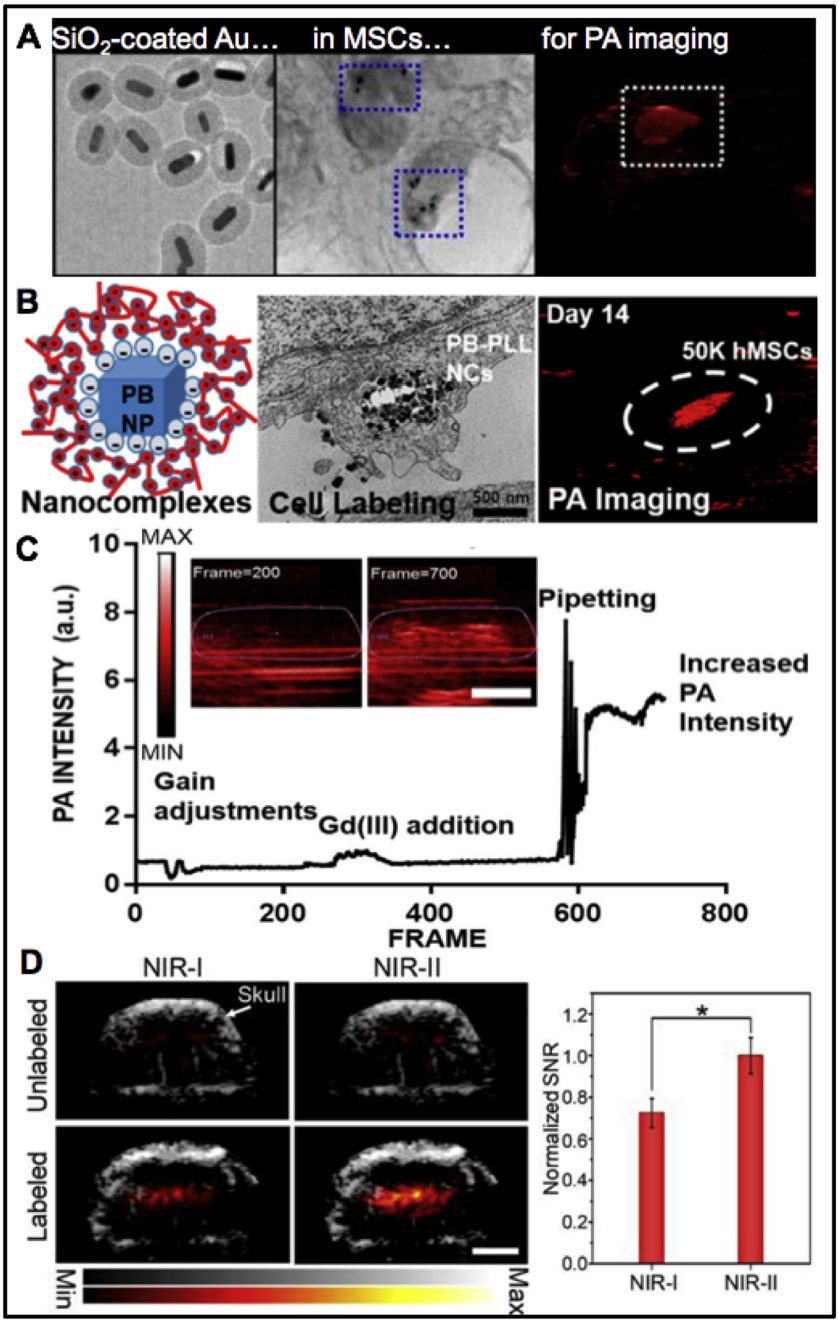

Fig. 6. Photoacoustic imaging of therapeutic stem cells. (A) Silica-coated gold nanorods were internalized by MSCs and enabled photoacoustic cell tracking. Reproduced courtesy of the ACS. (B) Poly-L-Lysine (PLL)-coated Prussian blue nanocubes were taken up by hMSCs and increased the photoacoustic contrast of hMSCs. Reproduced courtesy of the ACS. (C) Gadolinium doping increased the photoacoustic intensity of synthetic melanin nanoparticles. Reproduced courtesy of the ACS [122]. (D) Organic semiconducting polymer nanoparticles that can be excited in the second near-infrared window increased the photoacoustic signal-to-noise ratio compared to the first near-infrared window. Reproduced courtesy of the ACS [115,119,123].

laser diodes, etc.) could also accelerate clinical translation. At this stage, much work is still required to reveal the full potential of photoacoustics for theranostic drug delivery. For the near future, it is likely that strategies that are (1) surface-weighted and (2) leverage molecules with existing FDA approval, such as methylene blue and indocyanine green, will have the least regulatory burden for clinical translation. Finally, photoacoustic imaging may never become as prevalent as PET/CT for biodistribution and pharmacokinetics; however, it is highly adaptable for localized imaging and measurements without requiring any ionizing radiation. It drastically increases the contrast and potential for molecular imaging of ultrasound, which is already one of the most common modalities in medicine.

Acknowledgements

We acknowledge support from the National Institutes of Health through DP2 HL 137187 and T32 EB 009380.

References

[1] A. Webb, G.C. Kagadis, Introduction to biomedical imaging, Med. Phys. 30 (2003) 2267.
[2] T.F. Massoud, S.S. Gambhir, Molecular imaging in living subjects: seeing fundamental biological processes in a new light, Genes Dev. 17 (2003) 545–580.
[3] B. Shen, J. Jeon, M. Palner, D. Ye, A. Shuhendler, F.T. Chin, J. Rao, Positron emission tomography imaging of drug-induced tumor apoptosis with a caspase-triggered nanoaggregation probe, Angew. Chem. Int. Ed. 52 (2013) 10511–10514.

[4] W.J. Mulder, G.J. Strijkers, G.A. van Tilborg, A.W. Griffioen, K. Nicolay, Lipid-based nanoparticles for contrast-enhanced MRI and molecular imaging, NMR Biomed. 19 (2006) 142–164.
[5] H.B. Na, I.C. Song, T. Hyeon, Inorganic nanoparticles for MRI contrast agents, Adv. Mater. 21 (2009) 2133–2148.
[6] G. Liang, J. Ronald, Y. Chen, D. Ye, P. Pandit, M.L. Ma, B. Rutt, J. Rao, Controlled self-assembling of gadolinium nanoparticles as smart molecular magnetic resonance imaging contrast agents, Angew. Chem. Int. Ed. 50 (2011) 6283–6286.
[7] J.Y. Park, M.J. Baek, E.S. Choi, S. Woo, J.H. Kim, T.J. Kim, J.C. Jung, K.S. Chae, Y. Chang, G.H. Lee, Paramagnetic ultrasmall gadolinium oxide nanoparticles as advanced T 1 MRI contrast agent: account for large longitudinal relaxivity, optimal particle diameter, and in vivo T 1 MR images, ACS Nano 3 (2009) 3663–3669.
[8] T. Kim, E. Momin, J. Choi, K. Yuan, H. Zaidi, J. Kim, M. Park, N. Lee, M.T. McMahon, A. Quinones-Hinojosa, Mesoporous silica-coated hollow manganese oxide nanoparticles as positive T 1 contrast agents for labeling and MRI tracking of adipose-derived mesenchymal stem cells, J. Am. Chem. Soc. 133 (2011) 2955–2961.
[9] R. Qiao, C. Yang, M. Gao, Superparamagnetic iron oxide nanoparticles: from preparations to in vivo MRI applications, J. Mater. Chem. 19 (2009) 6274–6293.
[10] S.N. Reske, J. Kotzerke, FDG-PET for clinical use, Eur. J. Nucl. Med. 28 (2001) 1707–1723.
[11] S.M. Ametamey, M. Honer, P.A. Schubiger, Molecular imaging with PET, Chem. Rev. 108 (2008) 1501–1516.
[12] M.M. Khalil, J.L. Tremoleda, T.B. Bayomy, W. Gsell, Molecular SPECT Imaging: An Overview, International Journal of Molecular Imaging, 2011, 2011.
[13] J.A. Ronald, B.-S. Kim, G. Gowrishankar, M. Namavari, I.S. Alam, A. D'Souza, H. Nishikii, H.-Y. Chuang, O. Ilovich, C.-F. Lin, A PET imaging strategy to visualize activated T cells in acute graft-versus-host disease elicited by allogenic hematopoietic cell transplant, Cancer Res. 77 (2017) 2893–2902.
[14] F. Kiessling, S. Fokong, P. Koczera, W. Lederle, T. Lammers, Ultrasound microbubbles for molecular diagnosis, therapy, and theranostics, J. Nucl. Med. 53 (2012) 345–348.
[15] R. Deckers, C.T. Moonen, Ultrasound triggered, image guided, local drug delivery, J. Control. Release 148 (2010) 25–33.
[16] G.D. Luker, K.E. Luker, Optical imaging: current applications and future directions, J. Nucl. Med. 49 (2008) 1–4.
[17] A.G. Sorensen, Magnetic resonance as a cancer imaging biomarker, J. Clin. Oncol. 24 (2006) 3274–3281.
[18] S. Mitragotri, Healing sound: the use of ultrasound in drug delivery and other therapeutic applications, Nat. Rev. Drug Discov. 4 (2005) 255.
[19] L.V. Wang, S. Hu, Photoacoustic tomography: in vivo imaging from organelles to organs, Science (New York, N.Y.) 335 (2012) 1458–1462.
[20] J.E. Lemaster, J.V. Jokerst, What is new in nanoparticle-based photoacoustic imaging? Wiley Interdiscip. Rev. Nanomed. Nanobiotechnol. 9 (2017).
[21] C. Moore, J.V. Jokerst, Strategies for image-guided therapy, surgery, and drug delivery using photoacoustic imaging, Theranostics 9 (2019) 1550–1571.
[22] S. Zackrisson, S. Van De Ven, S. Gambhir, Light in and sound out: emerging translational strategies for photoacoustic imaging, Cancer Res. 74 (2014) 979–1004.
[23] A.G. Bell, The production of sound by radiant energy, Science (1881) 242–253.
[24] L.V. Wang, J. Yao, A practical guide to photoacoustic tomography in the life sciences, Nat. Methods 13 (2016) 627–638.
[25] J. Xia, J. Yao, L.V. Wang, Photoacoustic tomography: principles and advances, Electromagnetic Waves (Cambridge, Mass.) 147 (2014) 1–22.
[26] H.F. Zhang, K. Maslov, M. Sivaramakrishnan, G. Stoica, L.V. Wang, Imaging of hemoglobin oxygen saturation variations in single vessels in vivo using photoacoustic microscopy, Appl. Phys. Lett. 90 (2007), 053901.
[27] Y. Zhou, W. Xing, K.I. Maslov, L.A. Cornelius, L.V. Wang, Handheld photoacoustic microscopy to detect melanoma depth in vivo, Opt. Lett. 39 (2014) 4731–4734.
[28] B. Wang, A. Karpiouk, D. Yeager, J. Amirian, S. Litovsky, R. Smalling, S. Emelianov, Intravascular photoacoustic imaging of lipid in atherosclerotic plaques in the presence of luminal blood, Opt. Lett. 37 (2012) 1244–1246.
[29] B. Lan, W. Liu, Y.-c. Wang, J. Shi, Y. Li, S. Xu, H. Sheng, Q. Zhou, J. Zou, U. Hoffmann, W. Yang, J. Yao, High-speed widefield photoacoustic microscopy of small-animal hemodynamics, Biomed. Optics Express 9 (2018) 4689–4701.
[30] B. Ning, M.J. Kennedy, A.J. Dixon, N. Sun, R. Cao, B.T. Soetikno, R. Chen, Q. Zhou, K.K. Shung, J.A. Hossack, Simultaneous photoacoustic microscopy of microvascular anatomy, oxygen saturation, and blood flow, Opt. Lett. 40 (2015) 910–913.
[31] S. Mallidi, G.P. Luke, S. Emelianov, Photoacoustic imaging in cancer detection, diagnosis, and treatment guidance, Trends Biotechnol. 29 (2011) 213–221.
[32] G.P. Luke, D. Yeager, S.Y. Emelianov, Biomedical applications of photoacoustic imaging with exogenous contrast agents, Ann. Biomed. Eng. 40 (2012) 422–437.
[33] S.J. Arconada-Alvarez, J.E. Lemaster, J. Wang, J.V. Jokerst, The development and characterization of a novel yet simple 3D printed tool to facilitate phantom imaging of photoacoustic contrast agents, Photoacoustics 5 (2017) 17–24.
[34] Y. Jiang, K. Pu, Molecular fluorescence and photoacoustic imaging in the second near-infrared optical window using organic contrast agents, Adv. Biosys. 2 (2018) 1700262.
[35] E.C. Cho, C. Glaus, J. Chen, M.J. Welch, Y. Xia, Inorganic nanoparticle-based contrast agents for molecular imaging, Trends Mol. Med. 16 (2010) 561–573.
[36] Y. Jiang, K. Pu, Advanced photoacoustic imaging applications of near-infrared absorbing organic nanoparticles, Small 13 (2017) 1700710.
[37] J.V. Jokerst, D. Van de Sompel, S.E. Bohndiek, S.S. Gambhir, Cellulose nanoparticles are a biodegradable photoacoustic contrast agent for use in living mice, Photoacoustics 2 (2014) 119–127.
[38] L.V. Wang, S. Hu, Photoacoustic tomography: in vivo imaging from organelles to organs, Science 335 (2012) 1458–1462.
[39] L.R. Hirsch, R.J. Stafford, J. Bankson, S.R. Sershen, B. Rivera, R. Price, J.D. Hazle, N.J. Halas, J.L. West, Nanoshell-mediated near-infrared thermal therapy of tumors under magnetic resonance guidance, Proc. Natl. Acad. Sci. 100 (2003) 13549–13554.
[40] R.S. Riley, E.S. Day, Gold nanoparticle-mediated photothermal therapy: applications and opportunities for multimodal cancer treatment, Wiley Interdiscip. Rev. 9 (2017), e1449.
[41] P. Huang, J. Lin, W. Li, P. Rong, Z. Wang, S. Wang, X. Wang, X. Sun, M. Aronova, G. Niu, Biodegradable gold nanovesicles with an ultrastrong plasmonic coupling effect for photoacoustic imaging and photothermal therapy, Angew. Chem. Int. Ed. 52 (2013) 13958–13964.
[42] E.V. Shashkov, M. Everts, E.I. Galanzha, V.P. Zharov, Quantum dots as multimodal photoacoustic and photothermal contrast agents, Nano Lett. 8 (2008) 3953–3958.
[43] Z. Sheng, L. Song, J. Zheng, D. Hu, M. He, M. Zheng, G. Gao, P. Gong, P. Zhang, Y. Ma, Protein-assisted fabrication of nano-reduced graphene oxide for combined in vivo photoacoustic imaging and photothermal therapy, Biomaterials 34 (2013) 5236–5243.
[44] J.F. Lovell, C.S. Jin, E. Huynh, H. Jin, C. Kim, J.L. Rubinstein, W.C. Chan, W. Cao, L.V. Wang, G. Zheng, Porphysome nanovesicles generated by porphyrin bilayers for use as multimodal biophotonic contrast agents, Nat. Mater. 10 (2011) 324.
[45] Y. Lyu, Y. Fang, Q. Miao, X. Zhen, D. Ding, K. Pu, Intraparticle molecular orbital engineering of semiconducting polymer nanoparticles as amplified theranostics for in vivo photoacoustic imaging and photothermal therapy, ACS Nano 10 (2016) 4472–4481.
[46] L.-S. Lin, Z.-X. Cong, J.-B. Cao, K.-M. Ke, Q.-L. Peng, J. Gao, H.-H. Yang, G. Liu, X. Chen, Multifunctional Fe3O4@ polydopamine core–shell nanocomposites for intracellular mRNA detection and imaging-guided photothermal therapy, ACS Nano 8 (2014) 3876–3883.
[47] F. Gong, L. Cheng, N. Yang, Q. Jin, L. Tian, M. Wang, Y. Li, Z. Liu, Bimetallic oxide MnMoOX Nanorods for in vivo photoacoustic imaging of GSH and tumor-specific Photothermal therapy, Nano Lett. 18 (2018) 6037–6044.
[48] Y.-S. Chen, S.J. Yoon, W. Frey, M. Dockery, S. Emelianov, Dynamic contrast-enhanced photoacoustic imaging using photothermal stimuli-responsive composite nanomodulators, Nat. Commun. 8 (2017) 15782.
[49] Y. Lyu, J. Zeng, Y. Jiang, X. Zhen, T. Wang, S. Qiu, X. Lou, M. Gao, K. Pu, Enhancing both biodegradability and efficacy of semiconducting polymer nanoparticles for photoacoustic imaging and Photothermal therapy, ACS Nano 12 (2018) 1801–1810.
[50] W. Hongcharu, C.R. Taylor, D. Aghassi, K. Suthamjariya, R.R. Anderson, Y. Chang, Topical ALA-photodynamic therapy for the treatment of acne vulgaris, J. Investig. Dermatol. 115 (2000) 183–192.
[51] G.B. Kharkwal, S.K. Sharma, Y.Y. Huang, T. Dai, M.R. Hamblin, Photodynamic therapy for infections: clinical applications, Lasers Surg. Med. 43 (2011) 755–767.
[52] N. Bressler, Photodynamic therapy of subfoveal choroidal neovascularization in age-related macular degeneration with verteporfin: two-year results of 2 randomized clinical trials-tap report 2, Archives of Ophthalmol. (Chicago, Ill.: 1960) 119 (2001) 198–207.
[53] P. Agostinis, K. Berg, K.A. Cengel, T.H. Foster, A.W. Girotti, S.O. Gollnick, S.M. Hahn, M.R. Hamblin, A. Juzeniene, D. Kessel, Photodynamic therapy of cancer: an update, CA Cancer J. Clin. 61 (2011) 250–281.
[54] Y. Shen, A.J. Shuhendler, D. Ye, J.-J. Xu, H.-Y. Chen, Two-photon excitation nanoparticles for photodynamic therapy, Chem. Soc. Rev. 45 (2016) 6725–6741.
[55] C.J.H. Ho, G. Balasundaram, W. Driessen, R. McLaren, C.L. Wong, U.S. Dinish, A.B.E. Attia, V. Ntziachristos, M. Olivo, Multifunctional photosensitizer-based contrast agents for photoacoustic imaging, Sci. Rep. 4 (2014) 5342.
[56] N.M. Idris, M.K. Gnanasammandhan, J. Zhang, P.C. Ho, R. Mahendran, Y. Zhang, In vivo photodynamic therapy using upconversion nanoparticles as remote-controlled nanotransducers, Nat. Med. 18 (2012) 1580.
[57] P. Shao, D.W. Chapman, R.B. Moore, R.J. Zemp, Monitoring photodynamic therapy with photoacoustic microscopy, J. Biomed. Opt. 20 (2015) 106012.
[58] A. Srivatsan, S.V. Jenkins, M. Jeon, Z. Wu, C. Kim, J. Chen, R.K. Pandey, Gold nanocage-photosensitizer conjugates for dual-modal image-guided enhanced photodynamic therapy, Theranostics 4 (2014) 163.
[59] T. Liu, C. Wang, W. Cui, H. Gong, C. Liang, X. Shi, Z. Li, B. Sun, Z. Liu, Combined photothermal and photodynamic therapy delivered by PEGylated MoS2 nanosheets, Nanoscale 6 (2014) 11219–11225.
[60] W. Guo, Z. Qiu, C. Guo, D. Ding, T. Li, F. Wang, J. Sun, N. Zheng, S. Liu, Multifunctional theranostic agent of Cu2 (OH) PO4 quantum dots for photoacoustic image-guided photothermal/photodynamic combination cancer therapy, ACS Appl. Mater. Interfaces 9 (2017) 9348–9358.
[61] J. Hu, Y.A. Tang, A.H. Elmenoufy, H. Xu, Z. Cheng, X. Yang, Nanocomposite-based photodynamic therapy strategies for deep tumor treatment, Small 11 (2015) 5860–5887.
[62] N. Gupta, P. Price, E. Aboagye, PET for in vivo pharmacokinetic and pharmacodynamic measurements, Eur. J. Cancer 38 (2002) 2094–2107.
[63] A. Feis, C. Gellini, P.R. Salvi, M. Becucci, Photoacoustic excitation profiles of gold nanoparticles, Photoacoustics 2 (2014) 47–53.
[64] G.D. Moon, S.-W. Choi, X. Cai, W. Li, E.C. Cho, U. Jeong, L.V. Wang, Y. Xia, A new Theranostic system based on gold Nanocages and phase-change materials with unique features for photoacoustic imaging and controlled release, J. Am. Chem. Soc. 133 (2011) 4762–4765.
[65] K. Wilson, K. Homan, S. Emelianov, Biomedical photoacoustics beyond thermal expansion using triggered nanodroplet vaporization for contrast-enhanced imaging, Nat. Commun. 3 (2012) 618.

[66] A. Hannah, G. Luke, K. Wilson, K. Homan, S. Emelianov, Indocyanine Green-loaded photoacoustic Nanodroplets: dual contrast Nanoconstructs for enhanced photoacoustic and ultrasound imaging, ACS Nano 8 (2014) 250–259.
[67] J. Zhong, S. Yang, L. Wen, D. Xing, Imaging-guided photoacoustic drug release and synergistic chemo-photoacoustic therapy with paclitaxel-containing nanoparticles, J. Control. Release 226 (2016) 77–87.
[68] J. Zhong, S. Yang, X. Zheng, T. Zhou, D. Xing, In vivo photoacoustic therapy with cancer-targeted indocyanine green-containing nanoparticles, Nanomedicine 8 (2013) 903–919.
[69] J. Kang, D. Kim, J. Wang, Y. Han, J.M. Zuidema, A. Hariri, J.-H. Park, J.V. Jokerst, M.J. Sailor, Enhanced performance of a molecular photoacoustic imaging agent by encapsulation in mesoporous silicon nanoparticles, Adv. Mater. 30 (2018) 1800512.
[70] P. Manivasagan, S. Bharathiraja, N.Q. Bui, I.G. Lim, J. Oh, Paclitaxel-loaded chitosan oligosaccharide-stabilized gold nanoparticles as novel agents for drug delivery and photoacoustic imaging of cancer cells, Int. J. Pharm. 511 (2016) 367–379.
[71] G. Tian, X. Zhang, X. Zheng, W. Yin, L. Ruan, X. Liu, L. Zhou, L. Yan, S. Li, Z. Gu, Multifunctional RbxWO3 Nanorods for simultaneous combined chemo-photothermal therapy and photoacoustic/CT imaging, Small 10 (2014) 4160–4170.
[72] T. Bao, W. Yin, X. Zheng, X. Zhang, J. Yu, X. Dong, Y. Yong, F. Gao, L. Yan, Z. Gu, One-pot synthesis of PEGylated plasmonic MoO3–x hollow nanospheres for photoacoustic imaging guided chemo-photothermal combinational therapy of cancer, Biomaterials 76 (2016) 11–24.
[73] X.R. Song, X. Wang, S.X. Yu, J. Cao, S.H. Li, J. Li, G. Liu, H.H. Yang, X. Chen, Co9Se8 Nanoplates as a new Theranostic platform for photoacoustic/magnetic resonance dual-modal-imaging-guided chemo-Photothermal combination therapy, Adv. Mater. 27 (2015) 3285–3291.
[74] J. Liu, C. Wang, X. Wang, X. Wang, L. Cheng, Y. Li, Z. Liu, Mesoporous silica coated single-walled carbon nanotubes as a multifunctional light-responsive platform for cancer combination therapy, Adv. Funct. Mater. 25 (2015) 384–392.
[75] J. Song, X. Yang, O. Jacobson, L. Lin, P. Huang, G. Niu, Q. Ma, X. Chen, Sequential drug release and enhanced photothermal and photoacoustic effect of hybrid reduced graphene oxide-loaded ultrasmall gold nanorod vesicles for cancer therapy, ACS Nano 9 (2015) 9199–9209.
[76] P. Manivasagan, S. Bharathiraja, N.Q. Bui, B. Jang, Y.-O. Oh, I.G. Lim, J. Oh, Doxorubicin-loaded fucoidan capped gold nanoparticles for drug delivery and photoacoustic imaging, Int. J. Biol. Macromol. 91 (2016) 578–588.
[77] S. Duan, Y. Yang, C. Zhang, N. Zhao, F.-J. Xu, NIR-responsive Polycationic gatekeeper-cloaked hetero-nanoparticles for multimodal imaging-guided triple-combination therapy of Cancer, Small 13 (2017) 1603133.
[78] F. Coldur, M. Andac, All-solid-state polyvinyl chloride membrane lithium-selective electrode with improved selectivity and its application in serum lithium assay, Sens. Lett. 9 (2011) 1738–1744.
[79] R. Belmaker, Bipolar disorder, N. Engl. J. Med. 351 (2004) 476–486.
[80] K.J. Cash, C. Li, J. Xia, L.V. Wang, H.A. Clark, Optical drug monitoring: photoacoustic imaging of nanosensors to monitor therapeutic Lithium in vivo, ACS Nano 9 (2015) 1692–1698.
[81] I.-T. Ho, J.L. Sessler, S.S. Gambhir, J.V. Jokerst, Parts per billion detection of uranium with a porphyrinoid-containing nanoparticle and in vivo photoacoustic imaging, Analyst 140 (2015) 3731–3737.
[82] C. Qin, K. Cheng, K. Chen, X. Hu, Y. Liu, X. Lan, Y. Zhang, H. Liu, Y. Xu, L. Bu, X. Su, X. Zhu, S. Meng, Z. Cheng, Tyrosinase as a multifunctional reporter gene for photoacoustic/MRI/PET triple modality molecular imaging, Sci. Rep. 3 (2013) 1490.
[83] H.M. Hersi, N. Raulf, J. Gaken, N.D. Folarin, M. Tavassoli, MicroRNA-9 inhibits growth and invasion of head and neck cancer cells and is a predictive biomarker of response to plerixafor, an inhibitor of its target CXCR4, Mol. Oncol. 12 (2018) 2023–2041.
[84] H.F. Zheng, L. Zhou, Y.R. Shi, J. Tian, F. Wang, Tyrosinase-based reporter gene for photoacoustic imaging of MicroRNA-9 regulated by DNA methylation in living subjects, Mol Ther-Nucl Acids 11 (2018) 34–40.
[85] M.R. Buchanan, F.A. Ofosu, S.J. Brister, ThrombinIts Key Role in Thrombogenesis-Implications for Its Inhibition, CRC Press, 1994.
[86] P. Brill-Edwards, J.S. Ginsberg, M. Johnston, J. Hirsh, Establishing a therapeutic range for heparin therapy, Ann. Intern. Med. 119 (1993) 104–109.
[87] B.M. Reilly, R.A. Raschke, New method to predict patients' intravenous heparin dose requirements, J. Gen. Intern. Med. 11 (1996) 168–173.
[88] A. Liveris, R.A. Bello, P. Friedmann, M.A. Duffy, D. Manwani, J.S. Killinger, D. Rodriquez, S. Weinstein, Anti-factor Xa assay is a superior correlate of heparin dose than activated partial thromboplastin time or activated clotting time in pediatric extracorporeal membrane oxygenation*, Pediatr. Crit. Care Med. 15 (2014) e72–e79.
[89] K. Zmuda, D. Neofotistos, C.-H. Tsao, Effects of unfractionated heparin, low-molecular-weight heparin, and heparinoid on thromboelastographic assay of blood coagulation, Am. J. Clin. Pathol. 113 (2000) 725–731.
[90] G. Despotis, J. Joist, C. Hogue Jr., A. Alsoufiev, K. Kater, L. Goodnough, S. Santoro, E. Spitznagel, M. Rosenblum, D. Lappas, The impact of heparin concentration and activated clotting time monitoring on blood conservation: a prospective, randomized evaluation in patients undergoing cardiac operation, J. Thorac. Cardiovasc. Surg. 110 (1995) 46–54.
[91] J. Arimura, R.L. Poole, M. Jeng, W. Rhine, P. Sharek, Neonatal heparin overdose-a multidisciplinary team approach to medication error prevention, J. Pediat. Pharmacol. Therapeut. 13 (2008) 96–98.
[92] X. Wang, X. Xie, G. Ku, L.V. Wang, G. Stoica, Noninvasive imaging of hemoglobin concentration and oxygenation in the rat brain using high-resolution photoacoustic tomography, J. Biomed. Opt. 11 (2006), 024015.
[93] J. Wang, A.S. Jeevarathinam, K. Humphries, A. Jhunjhunwala, F. Chen, A. Hariri, B.R. Miller III, J.V. Jokerst, A mechanistic investigation of methylene blue and heparin interactions and their photoacoustic enhancement, Bioconjug. Chem. 29 (2018) 3768–3775.
[94] J. Wang, F. Chen, S.J. Arconada-Alvarez, J. Hartanto, L.-P. Yap, R. Park, F. Wang, I. Vorobyova, G. Dagliyan, P.S. Conti, A nanoscale tool for photoacoustic-based measurements of clotting time and therapeutic drug monitoring of heparin, Nano Lett. 16 (2016) 6265–6271.
[95] A.S. Jeevarathinam, N. Pai, K. Huang, A. Hariri, J. Wang, Y. Bai, L. Wang, T. Hancock, S. Keys, W. Penny, J.V. Jokerst, A cellulose-based photoacoustic sensor to measure heparin concentration and activity in human blood samples, Biosens. Bioelectron. 126 (2019) 831–837.
[96] T. Kim, Q. Zhang, J. Li, L. Zhang, J.V. Jokerst, A gold/silver hybrid nanoparticle for treatment and photoacoustic imaging of bacterial infection, ACS Nano 12 (2018) 5615–5625.
[97] M.L. Springer, R.E. Sievers, M.N. Viswanathan, M.S. Yee, E. Foster, W. Grossman, Y. Yeghiazarians, Closed-chest cell injections into mouse myocardium guided by high-resolution echocardiography, Am. J. Phys. Heart Circ. Phys. 289 (2005) H1307–H1314.
[98] M. Rodriguez-Porcel, O. Gheysens, I.Y. Chen, J.C. Wu, S.S. Gambhir, Image-guided cardiac cell delivery using high-resolution small-animal ultrasound, Mol. Ther. 12 (2005) 1142–1147.
[99] C. Bara, A. Ghodsizad, M. Niehaus, M. Makoui, C. Piechaczek, U. Martin, G. Warnecke, M. Karck, E. Gams, H.M. Klein, A. Haverich, A. Ruhparwar, In vivo echocardiographic imaging of transplanted human adult stem cells in the myocardium labeled with clinically applicable CliniMACS nanoparticles, J. Am. Soc. Echocardiogr. 19 (2006) 563–568.
[100] J. Hartanto, J.V. Jokerst, Nanoparticles for ultrasound-guided imaging of cell implantation, in: J.W.M. Bulte, M.M.J. Modo (Eds.), Design and Applications of Nanoparticles in Biomedical Imaging, Springer International Publishing, Cham 2017, pp. 299–314.
[101] J.V. Jokerst, C. Khademi, S.S. Gambhir, Intracellular aggregation of multimodal silica nanoparticles for ultrasound-guided stem cell implantation, Sci. Transl. Med. 5 (2013) 177ra135.
[102] J.W.M. Bulte, H.E. Daldrup-Link, Clinical tracking of cell transfer and cell transplantation: trials and tribulations, Radiology 289 (2018) 604–615.
[103] J.V. Frangioni, R.J. Hajjar, In vivo tracking of stem cells for clinical trials in cardiovascular disease, Circulation 110 (2004) 3378–3383.
[104] J. Wang, J.V. Jokerst, Stem cell imaging: tools to improve cell delivery and viability, Stem Cells Int. 2016 (2016) 9240652.
[105] J.E. Lemaster, J.V. Jokerst, What is new in nanoparticle-based photoacoustic imaging? Wiley Interdiscip. Rev. 9 (2017) e1404.
[106] W. Cui, S. Tavri, M.J. Benchimol, M. Itani, E.S. Olson, H. Zhang, M. Decyk, R.G. Ramirez, C.V. Barback, Y. Kono, R.F. Mattrey, Neural progenitor cells labeling with microbubble contrast agent for ultrasound imaging in vivo, Biomaterials 34 (2013) 4926–4935.
[107] M.A. Pysz, J.K. Willmann, Targeted contrast-enhanced ultrasound: an emerging technology in abdominal and pelvic imaging, Gastroenterology 140 (2011) 785–790.
[108] F. Chen, M. Ma, J. Wang, F. Wang, S.X. Chern, E.R. Zhao, A. Jhunjhunwala, S. Darmadi, H. Chen, J.V. Jokerst, Exosome-like silica nanoparticles: a novel ultrasound contrast agent for stem cell imaging, Nanoscale 9 (2017) 402–411.
[109] P.J. Kempen, S. Greasley, K.A. Parker, J.L. Campbell, H.-Y. Chang, J.R. Jones, R. Sinclair, S.S. Gambhir, J.V. Jokerst, Theranostic mesoporous silica nanoparticles biodegrade after pro-survival drug delivery and ultrasound/magnetic resonance imaging of stem cells, Theranostics 5 (2015) 631–642.
[110] F. Foroutan, J.V. Jokerst, S.S. Gambhir, O. Vermesh, H.-W. Kim, J.C. Knowles, Sol–gel synthesis and Electrospraying of biodegradable (P2O5)55–(CaO)30–(Na2O)15 glass Nanospheres as a transient contrast agent for ultrasound stem cell imaging, ACS Nano 9 (2015) 1868–1877.
[111] M.A. Kuliszewski, H. Fujii, C. Liao, A.H. Smith, A. Xie, J.R. Lindner, H. Leong-Poi, Molecular imaging of endothelial progenitor cell engraftment using contrast-enhanced ultrasound and targeted microbubbles, Cardiovasc. Res. 83 (2009) 653–662.
[112] R.W. Bourdeau, A. Lee-Gosselin, A. Lakshmanan, A. Farhadi, S.R. Kumar, S.P. Nety, M.G. Shapiro, Acoustic reporter genes for noninvasive imaging of microorganisms in mammalian hosts, Nature 553 (2018) 86.
[113] A. Lakshmanan, G.J. Lu, A. Farhadi, S.P. Nety, M. Kunth, A. Lee-Gosselin, D. Maresca, R.W. Bourdeau, M. Yin, J. Yan, C. Witte, D. Malounda, F.S. Foster, L. Schroder, M.G. Shapiro, Preparation of biogenic gas vesicle nanostructures for use as contrast agents for ultrasound and MRI, Nat. Protoc. 12 (2017) 2050–2080.
[114] M.G. Shapiro, P.W. Goodwill, A. Neogy, M. Yin, F.S. Foster, D.V. Schaffer, S.M. Conolly, Biogenic gas nanostructures as ultrasonic molecular reporters, Nat. Nanotechnol. 9 (2014) 311–316.
[115] J.V. Jokerst, M. Thangaraj, P.J. Kempen, R. Sinclair, S.S. Gambhir, Photoacoustic imaging of mesenchymal stem cells in living mice via silica-coated gold nanorods, ACS Nano 6 (2012) 5920–5930.
[116] C. Wang, X. Ma, S. Ye, L. Cheng, K. Yang, L. Guo, C. Li, Y. Li, Z. Liu, Protamine functionalized single-walled carbon nanotubes for stem cell labeling and in vivo Raman/magnetic resonance/photoacoustic triple-modal imaging, Adv. Funct. Mater. 22 (2012) 2363–2375.
[117] E.M. Donnelly, K.P. Kubelick, D.S. Dumani, S.Y. Emelianov, Photoacoustic image-guided delivery of Plasmonic-nanoparticle-labeled mesenchymal stem cells to the spinal cord, Nano Lett. 18 (2018) 6625–6632.
[118] S.Y. Nam, L.M. Ricles, L.J. Suggs, S.Y. Emelianov, In Vivo Ultrasound and Photoacoustic Monitoring of Mesenchymal Stem Cells Labeled with Gold Nanotracers, Plos One, 7, 2012.

[119] T. Kim, J.E. Lemaster, F. Chen, J. Li, J.V. Jokerst, Photoacoustic imaging of human mesenchymal stem cells labeled with Prussian blue-poly(l-lysine) Nanocomplexes, ACS Nano 11 (2017) 9022–9032.
[120] J.E. Lemaster, F. Chen, T. Kim, A. Hariri, J.V. Jokerst, Development of a Trimodal contrast agent for acoustic and magnetic particle imaging of stem cells, ACS App. Nano Mater. 1 (2018) 1321–1331.
[121] C.Y. Lin, F. Chen, A. Hariri, C.J. Chen, P. Wilder-Smith, T. Takesh, J.V. Jokerst, Photoacoustic imaging for noninvasive periodontal probing depth measurements, J. Dent. Res. 97 (2018) 23–30.
[122] J.E. Lemaster, Z. Wang, A. Hariri, F. Chen, Z. Hu, Y. Huang, C.V. Barback, R. Cochran, N.C. Gianneschi, J.V. Jokerst, Gadolinium doping enhances the photoacoustic signal of synthetic melanin nanoparticles: a dual modality contrast agent for stem cell imaging, Chem. Mater. 31 (2019) 251–259.
[123] C. Yin, G.H. Wen, C. Liu, B.G. Yang, S.E. Lin, J.W. Huang, P.C. Zhao, S.H.D. Wong, K.Y. Zhang, X.Y. Chen, G. Li, X.H. Jiang, J.P. Huang, K.Y. Pu, L.D. Wang, L.M. Bian, Organic semiconducting polymer nanoparticles for photoacoustic labeling and tracking of stem cells in the second near-infrared window, ACS Nano 12 (2018) 12201–12211.
[124] N.N. Nystrom, L.C.M. Yip, J.J.L. Carson, T.J. Scholl, J.A. Ronald, A human photoacoustic imaging reporter gene using the clinical dye indocyanine green, bioRxiv (2019) 537100.
[125] D. Van de Sompel, L.S. Sasportas, J.V. Jokerst, S.S. Gambhir, Comparison of deconvolution filters for photoacoustic tomography, PLoS One 11 (2016), e0152597.
[126] M.R. Zeiderman, D.E. Morgan, J.D. Christein, W.E. Grizzle, K.M. McMasters, L.R. McNally, Acidic pH-targeted chitosan-capped mesoporous silica coated gold nanorods facilitate detection of pancreatic tumors via multispectral optoacoustic tomography, ACS Biomater. Sci. Eng. 2 (2016) 1108–1120.
[127] Y. Jiang, K. Pu, Molecular fluorescence and photoacoustic imaging in the second near-infrared optical window using organic contrast agents, Adv. Biosys. 2 (2018) 1700262.
[128] A.M. Smith, M.C. Mancini, S. Nie, Bioimaging: second window for in vivo imaging, Nat. Nanotechnol. 4 (2009) 710.
[129] W. Roach, T. Johnson, B. Rockwell, Proposed maximum permissible exposure limits for ultrashort laser pulses, Health Phys. 76 (1999) 349–354.
[130] J.-E. Park, M. Kim, J.-H. Hwang, J.-M. Nam, Golden opportunities: Plasmonic gold nanostructures for biomedical applications based on the second near-infrared window, Small Methods 1 (2017) 1600032.
[131] G. Ku, M. Zhou, S. Song, Q. Huang, J. Hazle, C. Li, Copper sulfide nanoparticles as a new class of photoacoustic contrast agent for deep tissue imaging at 1064 nm, ACS Nano 6 (2012) 7489–7496.
[132] K.A. Homan, M. Souza, R. Truby, G.P. Luke, C. Green, E. Vreeland, S. Emelianov, Silver Nanoplate contrast agents for in vivo molecular photoacoustic imaging, ACS Nano 6 (2012) 641–650.
[133] K. Homan, S. Kim, Y.-S. Chen, B. Wang, S. Mallidi, S. Emelianov, Prospects of molecular photoacoustic imaging at 1064 nm wavelength, Opt. Lett. 35 (2010) 2663–2665.
[134] X.-D. Zhang, H. Wang, A.L. Antaris, L. Li, S. Diao, R. Ma, A. Nguyen, G. Hong, Z. Ma, J. Wang, S. Zhu, J.M. Castellano, T. Wyss-Coray, Y. Liang, J. Luo, H. Dai, Traumatic brain injury imaging in the second near-infrared window with a molecular fluorophore, Adv. Mater. 28 (2016) 6872–6879.
[135] Y. Sun, M. Ding, X. Zeng, Y. Xiao, H. Wu, H. Zhou, B. Ding, C. Qu, W. Hou, A. Er-Bu, Novel bright-emission small-molecule NIR-II fluorophores for in vivo tumor imaging and image-guided surgery, Chem. Sci. 8 (2017) 3489–3493.
[136] A.P. Jathoul, J. Laufer, O. Ogunlade, B. Treeby, B. Cox, E. Zhang, P. Johnson, A.R. Pizzey, B. Philip, T. Marafioti, Deep in vivo photoacoustic imaging of mammalian tissues using a tyrosinase-based genetic reporter, Nat. Photonics 9 (2015) 239.
[137] L. Peters, I. Weidenfeld, U. Klemm, A. Loeschcke, R. Weihmann, K.-E. Jaeger, T. Drepper, V. Ntziachristos, A.C. Stiel, Phototrophic purple bacteria as optoacoustic in vivo reporters of macrophage activity, Nat. Commun. 10 (2019) 1191.